Published in International Journal of Greenhouse Gas Control 19 (2013) 432–440

VLE data and modelling of aqueous N,N-diethylethanolamine (DEEA) solutions

Juliana G. M.-S. Monteiro[1], Diego D. D. Pinto[1], Syed A. H. Zaidy[1], Ardi Hartono[1], Hallvard F. Svendsen[1,*]

[1]Department of Chemical Engineering, Norwegian University of Science and Technology, N-7491 Trondheim, Norway

[*] Corresponding author: hallvard.svendsen@chemeng.ntnu.no

Phone: 73594100

Address: Kjemi IV*402 Sem Sælands vei 6

Department of Chemical Engineering

Norwegian University of Science and Technology

7491 Trondheim

Abstract

This work focuses on N,N-diethylethanolamine (DEEA), a tertiary amine relevant in the phase-change solvents context. Vapour liquid equilibrium data for CO_2 loaded aqueous solutions of DEEA are presented. These, along with data for pure DEEA and the binary system H_2O-DEEA available in literature, are represented by a model correlating the activity coefficients with the electrolyte non-random two-liquid (eNRTL) model. The model is shown to represent the experimental data well. The equilibrium model allows for simulating the regeneration of the solvent, thereby providing a measurement for the energy demand of the process. Experimental heat of absorption data presented by Kim (2009) are used to validate the predictions of the model.

Keywords: N,N-diethylethanolamine (DEEA); VLE; e-NRTL; CO_2 capture

1. Introduction

The research on amines used for CO_2 capture by absorption has recently focused on proposing novel solvents or solvent blends that can lead to lower energy requirements in the regeneration process. In this context, the reactive absorption of CO_2 by tertiary amine solutions has been investigated. As first proposed by Donaldson and Nguyen (1980), tertiary amines promote the reaction of hydration of CO_2, leading to bicarbonate formation. The heat of formation of bicarbonates is lower than that of carbamates (formed when using primary and secondary amines). Part of the steam required for amine regeneration stems from the heat of absorption of CO_2 into the desired amine solution. Kim and Svendsen (2011) have shown, in a study involving primary, secondary and tertiary amines, diamines, triamines and cyclic amines, that the tertiary amines give the lowest heats of absorption. If this can be combined with high equilibrium temperature sensitivity and thereby a low requirement also for stripping steam, this could constitute a major improvement to the absorption process. Blends of amines and phase change solvents are promising concepts when it comes to improving the performance of the for CO_2 absorption process (Aleixo et al., 2011; Raynal et al., 2011).

Liebenthal et al. (2013) show that capturing CO_2 using the phase changing blend of N,N-diethylethanolamine (DEEA) and 3-(methylamino)propylamine (MAPA) can lead to lower energy requirements than the MEA process. The 5M DEEA 2M MAPA blend forms two phases upon CO_2 loading, and after separation almost all the CO_2 is present in the lower phase, which is also rich in MAPA. The upper phase consists mainly of DEEA and needs not to be sent to the stripper (Ciftja et al., 2013). Regenerating only a fraction of the solution can lead to lower operational cost on the stripping side of the process. More details on the process are given by Liebenthal et al. (2013).

This work focuses on DEEA, a tertiary alkanolamine. First, vapour liquid equilibrium data for CO_2 loaded aqueous solutions of DEEA are presented. Then, data for pure DEEA and the binary system H_2O-DEEA presented by Hartono et al. (2013) are represented by a model correlating the activity coefficients with the NRTL model (Renon and Prausnitz, 1968). This information is used for deriving an equilibrium model for the ternary system. The model is shown to represent the experimental data well.

As the DEEA-CO_2-H_2O is an electrolyte system, the electrolyte non-random two-liquid (eNRTL) model described by Chen and Evans (1986) is applied for calculating activity coefficients in the liquid phase. The eNRTL is an excess Gibbs energy model and has a large number of parameters which need to be fitted using experimental data. For this purpose the

particle swarm optimization (PSO) algorithm (Kennedy and Eberhart, 1995). The PSO is a non-gradient based method and does not require initial guesses to start the optimization. The algorithm is initialized randomly, and has a random component in generating new candidate solutions. In this way it is able to escape local minima in the search for the global minimum.

The equilibrium model allows for simulating the regeneration of the solvent, thereby providing a measurement for the energy demand of the process. Experimental heat of absorption data presented by Kim (2009) are used to validate the predictions of the model.

Because the eNRTL is a local composition model, the interaction parameters estimated in this work are valid regardless of the composition of the solvent. Hence, obtaining a good model for the DEEA-CO_2-H_2O contributes to modeling the blended DEEA-MAPA-CO_2-H_2O system.

2. Materials and Methods

DEEA (CAS no. 100-37-8, purity ≥99%) was provided by Sigma-Aldrich and used without further purification. The aqueous solutions were prepared by dilution with distilled water. CO_2 (purity 99.99%) and N_2 (purity 99.6%) were provided by AGA Gas GmbH.

2.1 Low temperature equilibrium measurements

Vapor Liquid Equilibrium (VLE) data were measured for CO_2 loaded DEEA solutions. Data from 40ºC to 80ºC at atmospheric pressure were measured using a low temperature atmospheric vapor-liquid equilibrium apparatus, designed to operate at temperatures up to 80ºC. The apparatus consists of four 360 cm^3 glass flasks, placed in a thermostat box. The apparatus and the experimental procedure are detailed by Ma'mun et al. (2005). A scheme of the set-up is shown in **Figure 1**.

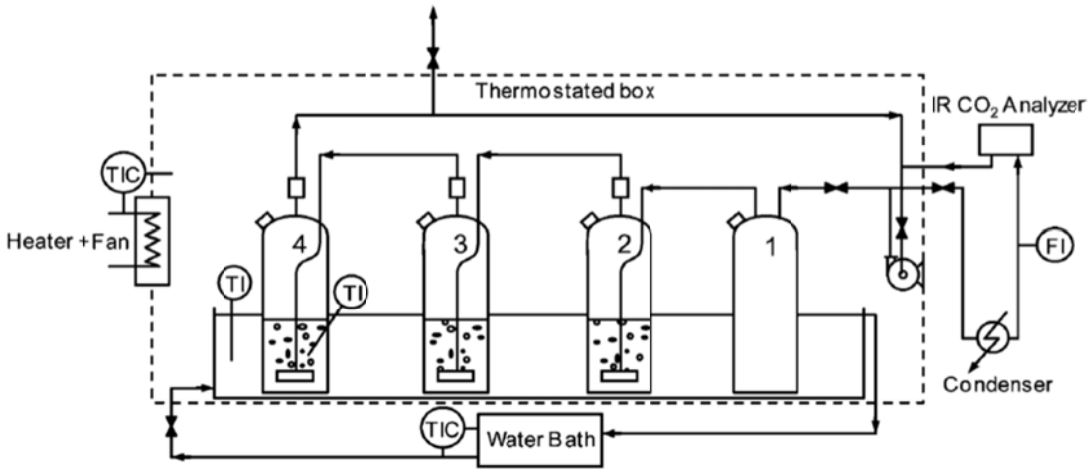

Figure 1 – Low temperature equilibrium set-up

The first flask was used a gas stabilizer, and the remaining three flasks were fed with 150 cm^3 of preloaded DEEA solutions each. The temperature in the thermostatic box was controlled using a water bath and measured with accuracy of 0.1 ºC. The gas phase from one flask is bubbled in the solution of the following flask, while the gas phase of the fourth flask is recirculated to the first flask. Equilibrium is reached within 20 min.

After equilibrium was obtained both gas and liquid phases were analyzed so that partial pressure of CO_2 and CO_2 loading could be determined. The gas sampling line was connected to a Rosemount BINOS® 100 CO_2 analyser, a non-dispersive infrared photometer. The instrument was calibrated before each use. Four different analysers channels were used, covering different concentration ranges: 0-2000ppm, 0-1%, 0-5% and 0-20%. The accuracy of the first three channels is of 0.01%, while the last channel has accuracy of 0.1%.

The CO_2 content in the liquid samples was determined in terms of mass of CO_2 per mass of solution by the so-called $BaCl_2$ method (Ma'mun, 2005). A known mass of a liquid sample was mixed with 50 ml sodium hydroxide (NaOH 0.1N) and 25 ml of barium chloride ($BaCl_2$ 0.1N) solutions. Upon heating, the barium carbonate ($BaCO_3$) precipitation is enhanced. After cooling, the precipitate was quantitatively filtered and totally dissolved in a solution of de-ionized water and a known mass of hydrochloric acid (HCl) 0.1N, added in excess. The excess of HCl was titrated with 0.1N solution of NaOH in an automatic titrator (Metrohm 702 Sm Titrino) with an end point of pH 5.2.

For loaded systems with high equilibrium pressure, the vapor-liquid equilibrium for the system was measured using a high temperature VLE apparatus. The measurements were taken

at 80ºC, 100ºC and 120ºC, and total pressure was measured as well as the corresponding liquid phase composition, using the $BaCl_2$ method.

The apparatus consists of two connected autoclaves (1000 and 200 cm^3), which rotate 180º at 2rpm and are designed to operate up to 2MPa and 150ºC. Druck PTX 610 (max 800kPa) and Schaevitz P 706-0025 (max 2.5 Mpa) pressure transducers, and two k-type thermocouples are used to record pressure and temperature. The autoclave is placed in a thermostated box heated by an oil bath. The autoclaves are purged with CO_2 and 200 cm^3 of unloaded DEEA solution of is injected into the smaller autoclave. CO_2 is injected to the desired pressure; equilibrium was obtained when temperature and pressure was constant to within ± 0.2 °C and ±1 kPa. This took approximately 3 to 8 hours. After equilibrium was obtained, a liquid sample is withdrawn from the smaller autoclave. A scheme of the set-up is given in

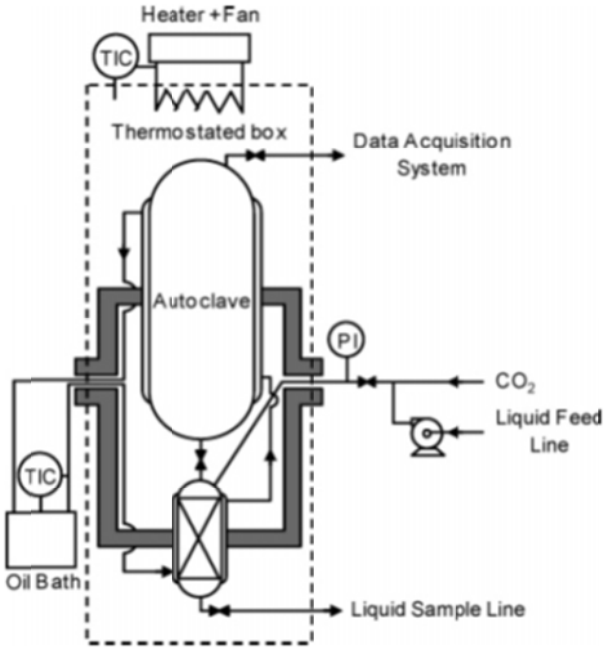

Figure 2

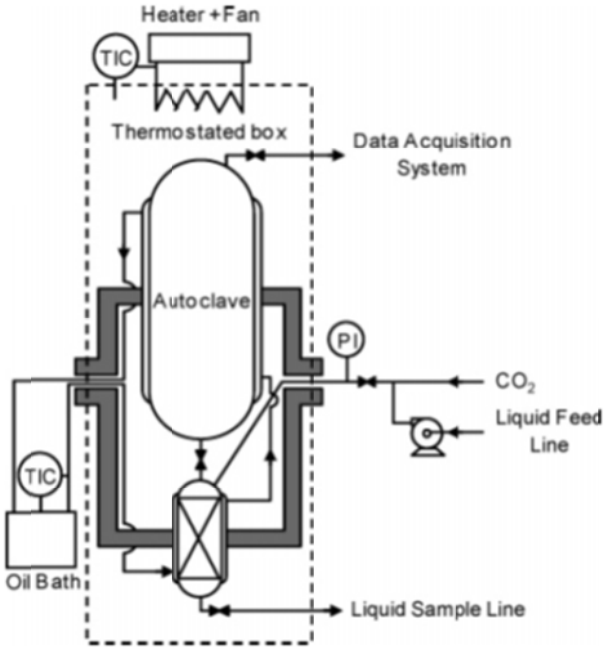

Figure 2 – High temperature equilibrium set-up

Since the DEEA solutions are prepared by weighing in DI water and pure amine, the initial content of DEEA is known. In order to verify that the total amine composition does not change during the experiments, initial and end liquid samples from all the experiments were analysed for amine content in terms of mass of DEEA per mass of solution. The DEEA content was determined by titration with 0.2N sulphuric acid (H_2SO_4) using an automatic titrator (Metrohm 702 Sm Titrino). The end point was obtained at a pH range from 3 to 4.

3. Experimental results

The data obtained are given from Table 1 to Table 4, for 2M (23.7wt %) and 5M (61.1wt %) DEEA solutions. The loadings were obtained from the liquid sample analyses and defined as the ratio of the number of moles of DEEA to the number of moles of CO_2 ($\alpha = mol_{CO_2} / mol_{DEEA}$).

Table 1 – Low VLE data for DEEA 2M

T = 40ºC		T = 60ºC		T = 80ºC	
Loading	**P_{CO2} (kPa)**	**Loading**	**P_{CO2} (kPa)**	**Loading**	**P_{CO2} (kPa)**
0.7716	9.246	0.684	17.342	0.346	12.1118
0.7821	9.860	0.599	11.162	0.326	10.8077
0.8215	16.091	0.600	11.167	0.307	9.0419

0.8105	12.901	0.612	11.423	0.286	8.1541
0.7905	10.353	0.552	9.167	0.259	7.0192
0.7268	6.530	0.497	6.533	0.219	5.1604
0.665	4.721	0.373	3.506	0.138	2.4091
0.610	3.194	0.260	1.736	0.113	1.5087
0.360	0.743	0.185	0.817	0.0472	0.2967
0.125	0.120	0.112	0.365	0.0283	0.1303
0.105	0.091	0.059	0.112		
0.0204	0.029	0.029	0.0448		

Table 2 – High VLE data for DEEA 2M

T = 80ºC		T = 100ºC		T = 120ºC	
Loading	**P (kPa)**	**Loading**	**P (kPa)**	**Loading**	**P (kPa)**
0.888	299.7	0.662	299.9	0.254	305.7
0.928	373.1	0.727	390.6	0.460	454.4
0.956	479.6	0.814	493.0	0.433	503.6
0.981	578.6	0.821	574.5	0.508	653.8
0.987	682.3	0.888	702.6	0.596	675.2
1.003	781.7	0.903	750.6	0.622	821.9
1.016	905.1	0.908	879.7	0.702	891.3
1.017	968.0	0.936	977.1	0.693	966.7
0.711	115.7	0.468	216.2	0.091	262.7

Table 3 – Low VLE data for DEEA 5M

T = 40ºC		T = 60ºC		T = 80ºC	
Loading	**P_{CO2} (kPa)**	**Loading**	**P_{CO2} (kPa)**	**Loading**	**P_{CO2} (kPa)**
0.3603	19.225	0.131	16.420	0.030	8.362
0.3359	16.124	0.106	11.962	0.036	11.875
0.3086	13.430	0.081	8.440	0.028	8.139
0.267	11.174	0.073	6.266	0.021	5.863
0.2573	10.295	0.056	4.331	0.017*	3.652
0.2253	8.303	0.042	3.325		
0.154	5.114	0.04	3.284		
0.112	3.133	0.034	2.501		
0.084	2.024	0.027	1.749		
0.046	0.668	0.014*	0.697		
0.033	0.471	0.008*	0.315		
0.032	0.483				
0.019*	0.327				
0.019*	0.307				
0.013*	0.192				
0.008*	0.112				
0.005*	0.078				
0.005*	0.063				

* Data removed in the second optimization

Table 4 – High VLE data for DEEA 5M

T = 80ºC		T = 100ºC		T = 120ºC	
Loading	**P (kPa)**	**Loading**	**P (kPa)**	**Loading**	**P (kPa)**
0.398	397.0	0.187	452.0	0.050	388.6
0.447	465.5	0.182	461.6	0.069	472.3
0.522	564.9	0.219	556.3	0.096	619.7
0.569	662.4	0.243	671.8	0.108	704.4
0.624	782.9	0.269	760.5	0.118	761.9
0.673	995.1	0.336	882.5	0.138	886.8
0.304	277.8	0.386	992.1	0.158	1035.3
0.253	223.5	0.100	273.3	0.012*	233.0
		0.057	176.6	0.0057*	212.1

* Data removed in the second optimization

4. The PSO algorithm

Kennedy and Eberhart (1995) first presented the PSO algorithm as an optimization tool in 1995. Although it was first introduced for simulation of social behaviour, this method gained attention from other fields and several modifications and implementations can now be found in literature. An extensive review of the PSO method is given by Poli et al. (2007).

The PSO dynamics is simple: the candidate solutions vectors, $\overline{p}_i$, are randomly initialized; $i \in [i, n_s]$. The provisional value for each parameter is within a pre-defined range, $\overline{A} \le \overline{p}_i \le \overline{B}$. In the PSO original article (Kennedy and Eberhart, 1995), these candidate solutions are referred to as *particles*, and a *swarm* is defined as a set of particles. The size of the swarm is then the number of candidate solution vectors, n_s. The objective function is evaluated for each $\overline{p}_i$ and the elements of each vector are then updated according to a relationship that takes into consideration the value of the objective function obtained for all the candidate solutions in the search of the minimum of the objective function. This relationship is the so-called interaction of the particles with their neighbours, and is set in order to mimic the social behaviour of a swarm. The interaction, often called topology, plays an important role in convergence. There are, basically, two types of topologies: (i) the *gbest* topology and (ii) the *lbest* topology. The *gbest*

topology considers $\overline{p}_i$ as a neighbour to all $\overline{p}_{j\neq i}$. This can lead to premature or false convergence in multi-modal fitness landscapes. To overcome this, in the *lbest* topology, a neighbouring logic is adopted so that only a set of vectors $\overline{p}_{j\neq i}$ is considered as a neighbour to $\overline{p}_i$. Among the different configurations of fixed neighbourhoods are the circle and the star geometries. However, variable random topologies are preferable, since they are shown to be more robust than fixed topologies (Ghosh et al., 2012). While the *lbest* topology is better suited to avoid local minimums, its convergence is slower than the *gbest* topology (Poli et al., 2007). In this work, the *lbest* topology with variable random neighbourhood is chosen.

The PSO algorithm can be described in 8 steps.

Step 1: Define the size of the set of candidate solutions vectors (swarm size, n_s), the inertia weight (ω), parameters ϕ_1 and ϕ_2, the number of maximum iterations, the tolerance and a probability threshold.

Step 2: randomly initialize the candidate solutions vectors (particles, $\overline{p}_i$) with values within a pre-defined range, $\overline{A} \leq \overline{p}_i \leq \overline{B}$.

$\overline{p}_i = [x_{i,1} \quad x_{i,2} \quad ... \quad x_{i,n\theta}]$ where $n\theta$ is the number of parameters to be optimized.

Step 3: calculate the objective function value $f^t(\overline{p}_i) \qquad i = 1,\ 2,\ ...,n_s$, where t denotes the t-th iteration,

Step 4: compare the objective function value $f^t(\overline{p}_i)$ with the minimum value obtained by $\overline{p}_i$, $f(\overline{p}_i^l)$. The value $\overline{p}_i^l$ is referred to as the particle's best position, and is the best set of parameters composing $\overline{p}_i$. If $f^t(\overline{p}_i) < f(\overline{p}_i^l)$ update the "best position" by setting $\overline{p}_i^l = \overline{p}_i$.

Step 5: for every $\overline{p}_i$, associate a randomly generated number within the interval [0,1] to every $\overline{p}_{j\neq i}$. If the number is smaller than this probability threshold, the particles are considered neighbours. The neighbourhood is designed by Λ and $\overline{p}_i$ and $\overline{p}_{j\neq i}$ are neigbours if $j \in \Lambda$.

Step 6: compare the function value $f^t\left(\overline{p}_i\right)$ with the neighbourhood values $f^t\left(\overline{p}_{j\neq i,\, j\in\Lambda}\right)$. The smallest value is the local best ($\overline{p}_i^g$).

Step 7: Update the parameter values ("positions") and velocities (equations 1 to 3).

Step 8: If the criteria are not fulfilled repeat steps 3 to 7. Else, print the results.

The procedure to update the parameter values within a candidate solution vector (or to a particle's position) is given by equation 1. The "velocities" are updated according to equation 2. if the *i*-particle is not in the best position in its neighbourhood or equation 3, if it is. Parameters φ_1 and φ_1 are random generators $\in\left[0,\phi_1\right]$ and $\in\left[0,\phi_2\right]$, respectively.

$$x_i^{t+1} = x_i^t + v_i^{t+1} \qquad (1)$$

$$v_i^{t+1} = wv_i^t + \varphi_1\left(p_i^l - x_i^t\right) + \varphi_2\left(p_i^g - x_i^t\right), \qquad p_i^l \neq p_i^g \qquad (2)$$

$$v_i^{t+1} = wv_i^t + \varphi_1\left(p_i^l - x_i^t\right), \qquad p_i^l = p_i^g \qquad (3)$$

5. Thermodynamic equilibrium modelling

The phase equilibrium between vapor and liquid phase can be expressed by equation 4 (Austgen et al., 1991).

$$py_i\phi_i = \Omega_i x_i \gamma_i \Psi_i \qquad (4)$$

where p is the system pressure [Pa], y_i and x_i are respectively the component *i* vapor and liquid mol fractions [-], ϕ_i is the fugacity coefficient [-] calculated using the Peng Robinson EoS and γ_i is the activity coefficient [-] calculated either by the NRTL or the e-NRTL model. The

function Ω_i [Pa] is dependent on the component reference state and is defined in equation 5. The infinite dilution reference state is used for CO_2, whereas water and DEEA are in the pure component reference state. The Poynting factor, Ψ_i [-], is also taken into account.

$$\Omega_i = \begin{cases} p_i^{sat}\phi_i^{sat}, \text{ pure component reference state} \\ H_i^{\infty}, \text{infinite dilution reference state} \end{cases} \quad \textbf{5}$$

where p_i^{sat} is the component vapour pressure [Pa], ϕ_i^{sat} is the component's fugacity coefficient, calculated at p_i^{sat}, and H_i^{∞} is the components Henry's constant at infinite dilution in water. The correlations and parameters for calculating p_i^{sat} and H_i^{∞} are given in Table 5.

In the Peng Robinson EoS model, the parameters of binary interaction between the molecules are set to zero, while their critical properties are retrieved from Yaws and Narasimhan (2009). The error generated by setting the interaction parameters to zero is compensated by regressing the parameters of the activity coefficient models against the experimental data.

In the e-NRTL model, the excess Gibbs energy is described as a sum of two contributions: short range and long range interactions (Chen and Evans, 1986). The long range interactions are due to electrostatic forces and are therefore only present in electrolyte systems. This work adopts the model presented by Austgen et al. (1989), in which the long-range term is represented by a Pitzer-Debye-Hückel term corrected by a Born term.

The short range interactions are described as function of non-randomness and energy parameters, which may vary with temperature. The expressions for calculating the activity coefficients as a function of these parameters can be found in Renon and Prausnitz (1968), for the NRTL model and in Chen and Evans (1986), for the electrolyte version. In this work, the PSO algorithm is used for fitting the parameters

5.1 H_2O-DEEA System

The unloaded aqueous DEEA system was assumed to be non-reactive; therefore, the NRTL model (Renon and Prausnitz, 1968) was chosen to model the activity coefficients in this binary system. VLE data presented by Hartono et al. (2013) and excess enthalpy data from Mathonat et al. (1997) were taken into account in the regression of the model parameters.

The non-randomness parameters of the NRTL model were optimized together with the energy parameters. As in Hessen (2010), the energy parameters were given a temperature dependency as shown by equation 6.

$$\tau_{ij} = a_{ij} + \frac{b_{ij}}{T} \qquad \textbf{6}$$

As can be seen from Figure 3, the model is able to represent well both pressure and excess enthalpy data. In Figure 4, the pressure data at low DEEA concentration are presented in detail. It is possible to observe that the model also predicts the azeotropes formed in the low DEEA concentration region. The objective function used is presented in equation 7 (Weiland et al., 1993).

$$F_{Obj} = \sum_{i=k}^{N} \frac{\left(\eta_k - \varphi_k\right)^2}{\left|\eta_k \varphi_k\right|} \qquad \textbf{7}$$

where N is the number of experimental points, φ_k is an experimental value and η_k is its value as predicted by the model.

The errors are reported separately for each property, in terms of averaged absolute relative deviation, AARD, as defined in equation 5. The obtained AARDs were 0.7% for total pressure, 0.24% for water vapor mole fraction, 7.0% for DEEA vapor mole fraction and 3.8% for excess enthalpy. The activity coefficients, presented in Figure 5, show the high non-ideality of this system at very low DEEA concentrations.

$$AARD[\%] = \frac{1}{N} \sum_{i=k}^{N} 100 \frac{\left|\eta_k - \varphi_k\right|}{\left|\varphi_k\right|} \qquad \textbf{8}$$

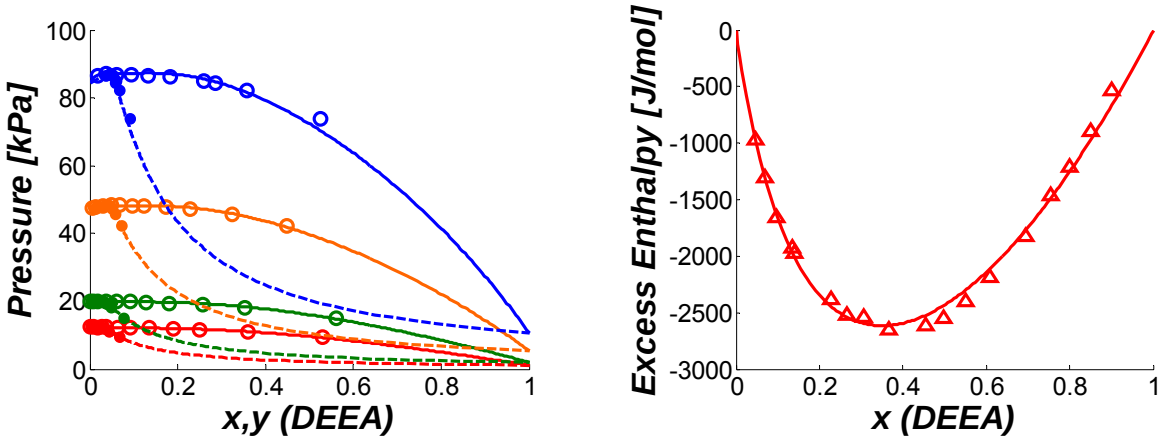

Figure 3 – Left: phase envelope (Pxy) diagram. Lines: model predictions, open points (○): x_{DEEA} experimental data, filled points (●) y_{DEEA} experimental data. Colours: 95ºC (blue), 80ºC (orange), 60ºC (green) and 50ºC (red); Right: excess enthalpy as a function of composition. Line: model predictions, Δ: experimental data from Mathonat *et al*. (1997) at 25ºC.

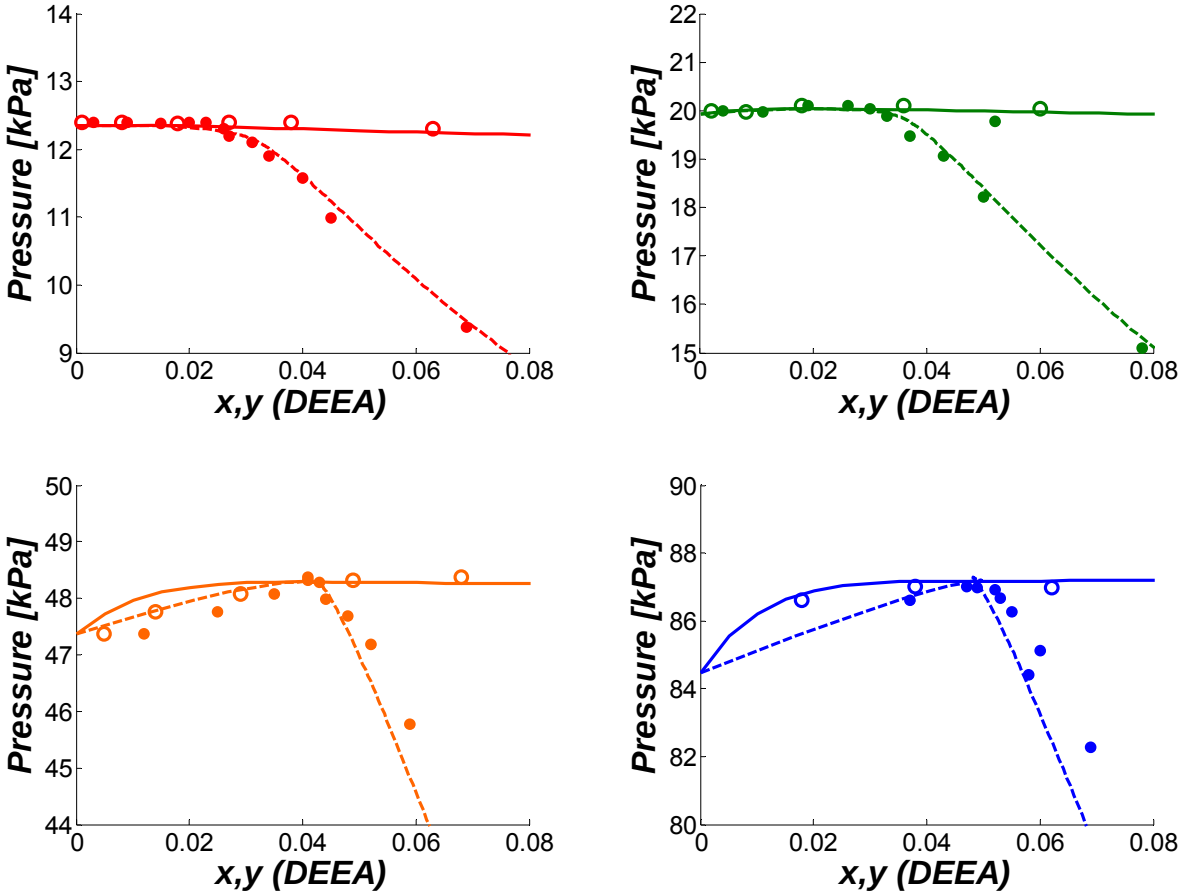

Figure 4 – Detail of the phase envelope (Pxy) diagrams at low DEEA concentrations. Lines: model predictions, open points (○): x_{DEEA} experimental data, filled points (●) y_{DEEA} experimental data. Upper left: 50ºC, upper right: 60ºC, lower left: 80ºC, lower right: 95ºC.

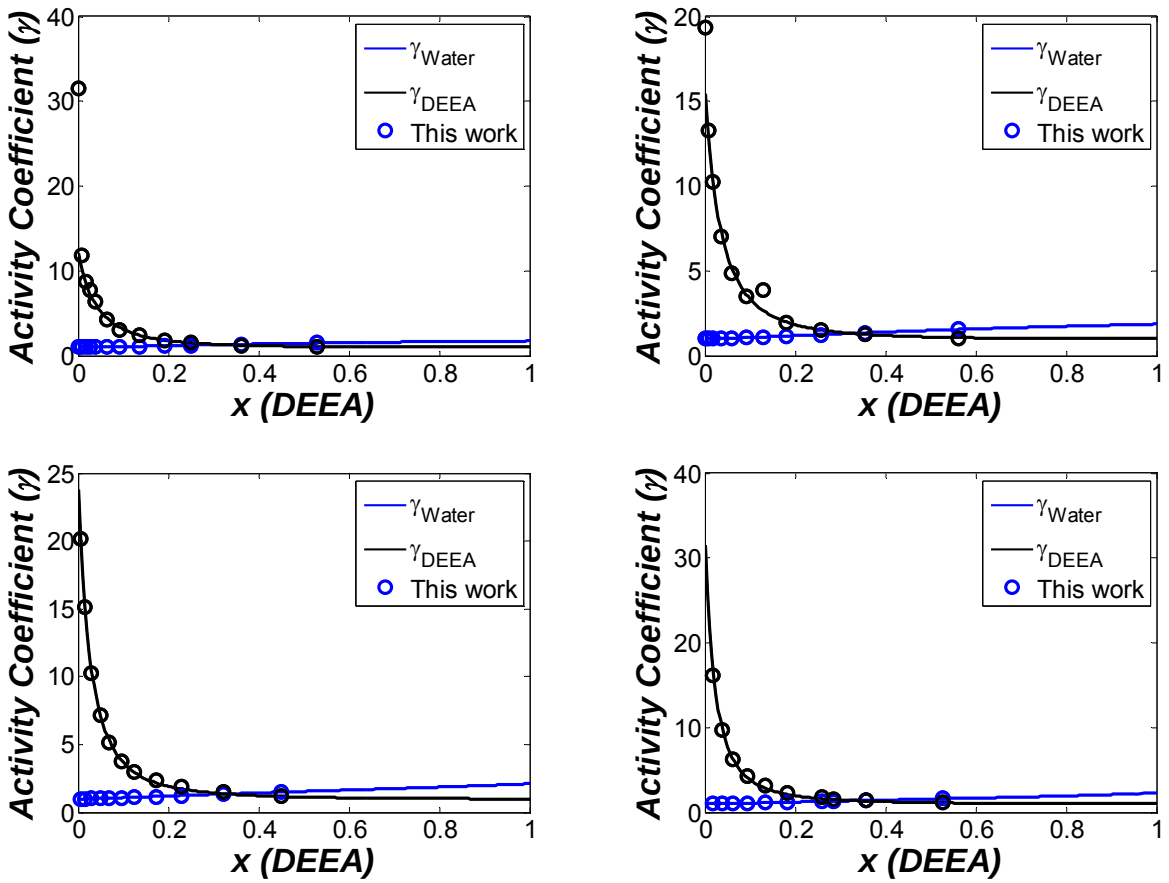

Figure 5 – Activity coefficients as a function of composition. Lines: model predictions, open points (○): experimental data. Colour code: water (blue), DEEA (black). Upper left: 50ºC, upper right: 60ºC, lower left: 80ºC, lower right: 95ºC.

5.2 The DEEA-H_2O-CO_2 system

The loaded aqueous DEEA system was modelled as a reactive system and the e-NRTL model (Chen and Evans, 1986) was chosen to model the activity coefficients. The VLE data presented in this work were taken into account in the regression of the model parameters.

According to Hessen et al. (2010), the non-randomness parameters of the e-NRTL model were fixed as 0.2 for the H_2O-salt pairs and as 0.1 for amine/CO_2-salt pairs. The molecule-molecule non-randomness parameters were fixed at 0.2, apart from the H_2O-DEEA and DEEA-H_2O parameters which were optimized as described in the previous section. The temperature-

dependent energy parameters were modelled according to equation 6. As in Pinto et al. (2013), the parameters of the H_2O-CO_2 system were fixed as the Aspen plus e-NRTL default values. The parameter values are given in Table 6.

As first proposed by Donaldson and Nguyen (1980), tertiary amines promote the reaction of hydration of CO_2, leading to bicarbonate formation, as in equation 6

$$DEEA + H_2O + CO_2 = DEEAH^+ + HCO_3^- \quad (6)$$

The reactions taking place in the system are described as follows:

$$2H_2O = H_3O^+ + OH^- \quad (7)$$

$$2H_2O + CO_2 = H_3O^+ + HCO_3^- \quad (8)$$

$$H_2O + HCO_3^- = H_3O^+ + CO_3^= \quad (9)$$

$$DEEA + H_3O^+ = DEEAH^+ + H_2O \quad (10)$$

Equation 6 is thereby described as the sum of reactions 8 and 10. Hence, there are 8 species present in the system, namely: (molecules) H_2O, CO_2, DEEA, (cations) H_3O^+, $DEEAH^+$ and (anions) OH^-, HCO_3^- and $CO_3^=$. The chemical equilibrium is solved by using the non-stoichiometric method, as in Hessen et al. (2010). The chemical equilibrium constants for each reaction are presented in Table 5.

In a first attempt, all the data presented in this work were used in the optimization of the eNRTL parameters. The obtained AARD were 18.6% for partial pressure of CO_2 and 10.2% for total pressure data. However, a great deal of the deviation is due to the scatter of the data at very low loadings. This is explained by the high relative uncertainty in the loading value itself in this region, since the errors in the analytical method used to determine the amount of CO_2 are high when the CO_2 content is low.

In order to ensure that the model is not greatly affected by the uncertainties, a second regression was performed taking into consideration only the points with loading equal to or higher than 0.02. This led to a considerable reduction in the obtained AARD: 15.5% for partial pressure of CO_2 and 8.1% for total pressure. The data removed in this second optimization are indicated in Table 1 to Table 4 with a star. The results shown in Figure 6 and Figure 7 are related to this second optimization. The data not used in the optimizations are also included.

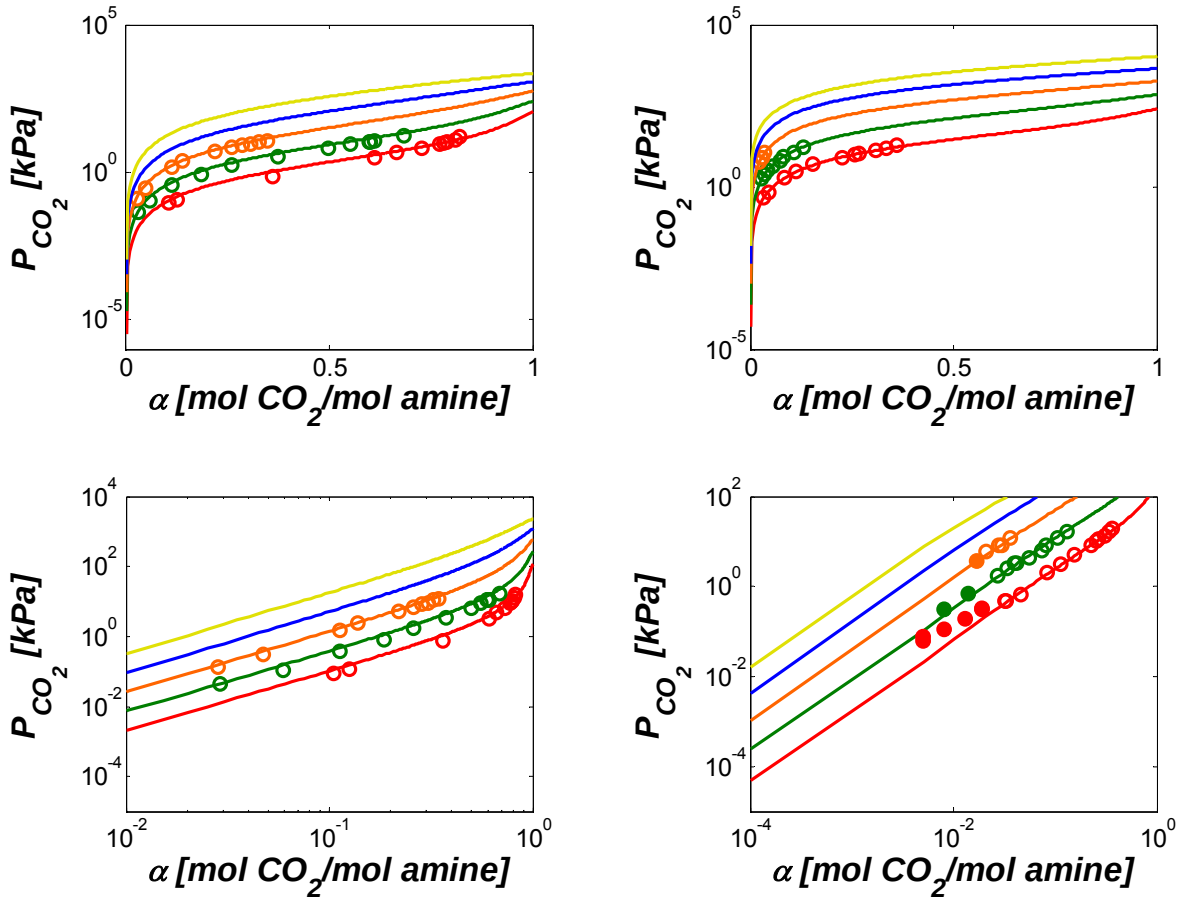

Figure 6 – CO_2 partial pressure. Lines: model predictions, open points (○): experimental data used in the regression, filled points (●) experimental data excluded from the regression. Colours: 120ºC (yellow), 100ºC (blue), 80ºC (orange), 60ºC (green) and 40ºC (red). Upper left: 2M in log-normal scale; upper right: 5M in log-normal; lower left: 2M in log-log scale; lower right: 5M in log-log scale.

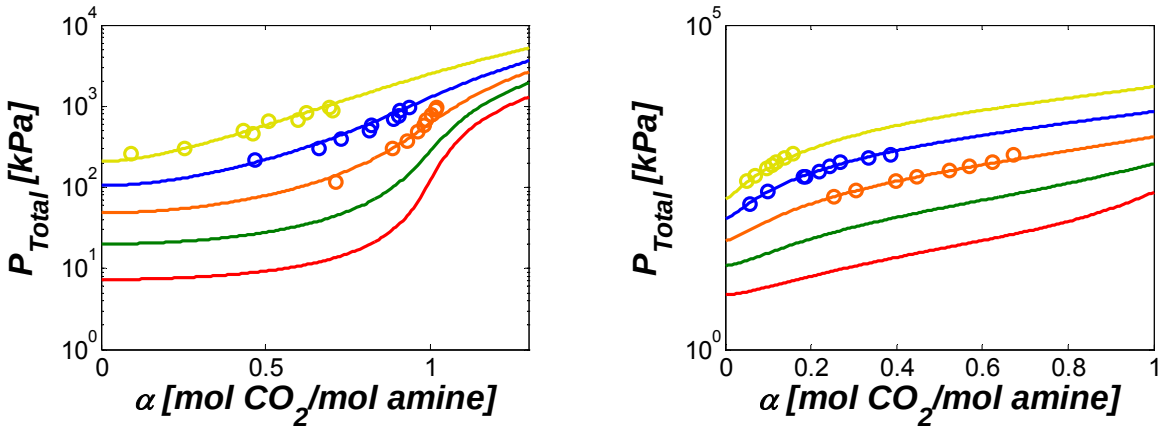

Figure 7 – Total pressure. Lines: model predictions, open points (○): experimental data used in the regression. Colours: 120ºC (yellow), 100ºC (blue), 80ºC (orange), 60ºC (green) and 40ºC (red). Left: 2M; right: 5M.

The model was used to predict heat of absorption values according to the procedure described by Kim et al. (2009). The model is compared to the values by Kim (2009) and results are shown in Figure 8. There is reasonably good agreement between the model and experimental data at 40ºC. However, the data at 80ºC are under-predicted by the model.

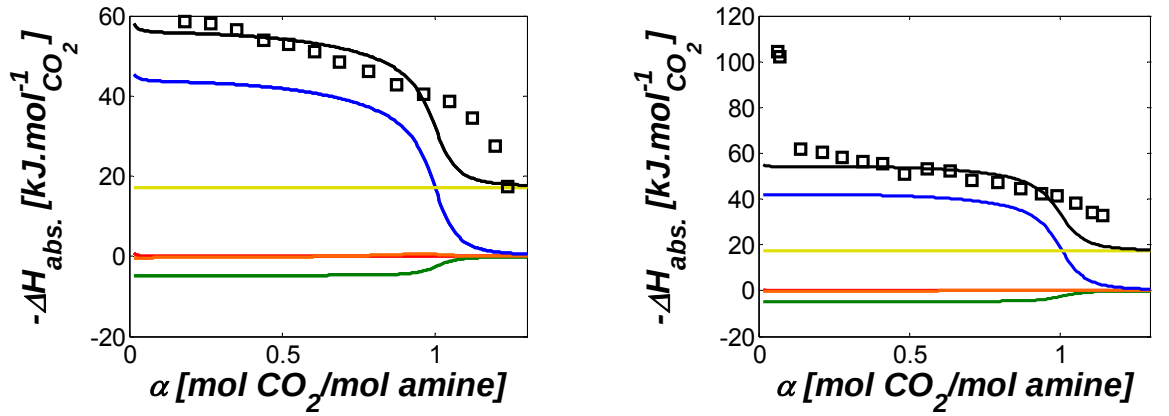

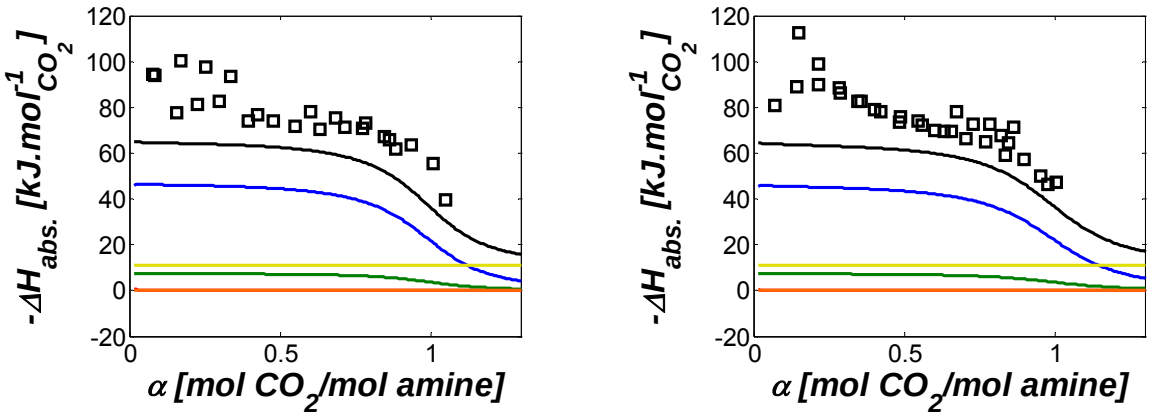

Figure 8 – Enthalpy of absorption. Lines: model predictions, open points (□): experimental data from Kim (2009). Upper left: 40ºC 32wt% DEEA, upper right 40ºC 37wt% DEEA, lower left: 80ºC 32wt% DEEA, lower right 80ºC 37wt% DEEA. Colours: black: total heat of absorption, blue: reaction 10, red: reaction 7; green: reaction 8; orange: reaction 9; yellow: CO_2 dissolution.

Table 5 – Constants used in the modeling[1].

$$\ln\left(K_{eq}\right) = A + B/T + C\ln\left(T\right) + D.T, \quad T \ in\ K$$

Reaction	A	B	C	D	Source
7	132.899	-13445.9	-22.4773	0	Edwards et al. (1978)
8	231.465	-12092.1	-36.7816	0	Edwards et al. (1978)
9	216.049	-12431.7	-35.4819	0	Edwards et al. (1978)
10	-110.8649	90.5882	14.5518	0.0039	This work[2]

$$\ln\left(p_i^{sat}\right) = A + B/T + C\ln\left(T\right) + DT^E, \quad p_i^{sat}\ in\ Pa,\ and\ T\ in\ K$$

Component	A	B	C	D	E	Source
H_2O	73.649	-7258.2	-7.3037	4.1653E-06	2	DIPPR (2004)

$$\log_{10}\left(p_i^{sat}\right) = A + B/T + C, \quad p_i^{sat}\ in\ Pa,\ and\ T\ in\ K$$

Component	A	B	C	Source
DEEA	9.2446	-1512.465	-78.2565	This work[3]

$$\ln\left(H_{CO_2}^{\infty}\right) = A + B/T + C/T^2 + D/T^3, \quad H_{CO_2}^{\infty}\ in\ MPa,\ and\ T\ in\ K$$

Component	A	B * 10^{-4}	C * 10^{-6}	D * 10^{-8}	Source
CO_2	-6.8346	1.2817	-3.7668	2.997	Carroll et al. (1991)

[1]Chemical equilibrium constant given in mol fraction basis.

[2]Asymmetric reference state, fitted in this work using data from Hamborg and Versteeg (2009).

[3]Fitted in this work using data from Hartono et al. (2013)

Table 6 – e-NRTL parameters.

Molecular Parameters: a_{mm}, b_{mm}			
a_{H_2O,CO_2}	0*	b_{H_2O,CO_2}	0*
$a_{H_2O,DEEA}$	7.8624**	$b_{H_2O,DEEA}$	-1720.550**
a_{CO_2,H_2O}	0*	b_{CO_2,H_2O}	0*
$a_{CO_2,DEEA}$	0.1739	$b_{CO_2,DEEA}$	-865.699
a_{DEEA,H_2O}	2.8797**	b_{DEEA,H_2O}	-945.299**
a_{DEEA,CO_2}	3.5452	b_{DEEA,CO_2}	509.611
Molecule-Salt Parameters: $a_{m,c/a}$, $b_{m,c/a}$			
$a_{H_2O,H_3O^+/OH^-}$	8*	$b_{H_2O,H_3O^+/OH^-}$	0*
$a_{H_2O,H_3O^+/HCO_3^-}$	8*	$b_{H_2O,H_3O^+/HCO_3^-}$	0*
$a_{H_2O,H_3O^+/CO_3^=}$	8*	$b_{H_2O,H_3O^+/CO_3^=}$	0*
$a_{H_2O,DEEAH^+/OH^-}$	6.4195	$b_{H_2O,DEEAH^+/OH^-}$	51.2782
$a_{H_2O,DEEAH^+/HCO_3^-}$	-4.0053	$b_{H_2O,DEEAH^+/HCO_3^-}$	311.364

$a_{H_2O,DEEAH^+/CO_3^=}$	-5.0000	$b_{H_2O,DEEAH^+/CO_3^=}$	-93.261
$a_{CO_2,H_3O^+/OH^-}$	15*	$b_{CO_2,H_3O^+/OH^-}$	0*
$a_{CO_2,H_3O^+/HCO_3^-}$	15*	$b_{CO_2,H_3O^+/HCO_3^-}$	0*
$a_{CO_2,H_3O^+/CO_3^=}$	15*	$b_{CO_2,H_3O^+/CO_3^=}$	0*
$a_{CO_2,DEEAH^+/OH^-}$	12.3239	$b_{CO_2,DEEAH^+/OH^-}$	-312.476
$a_{CO_2,DEEAH^+/HCO_3^-}$	8.3840	$b_{CO_2,DEEAH^+/HCO_3^-}$	608.436
$a_{CO_2,DEEAH^+/CO_3^=}$	-2.7114	$b_{CO_2,DEEAH^+/CO_3^=}$	-527.063
$a_{DEEA,H_3O^+/OH^-}$	5.3103	$b_{DEEA,H_3O^+/OH^-}$	-320.665
$a_{DEEA,H_3O^+/HCO_3^-}$	3.5081	$b_{DEEA,H_3O^+/HCO_3^-}$	-602.792
$a_{DEEA,H_3O^+/CO_3^=}$	3.1376	$b_{DEEA,H_3O^+/CO_3^=}$	-282.638
$a_{DEEA,DEEAH^+/OH^-}$	8.3121	$b_{DEEA,DEEAH^+/OH^-}$	-509.234
$a_{DEEA,DEEAH^+/HCO_3^-}$	4.6737	$b_{DEEA,DEEAH^+/HCO_3^-}$	-410.104
$a_{DEEA,DEEAH^+/CO_3^=}$	8.3565	$b_{DEEA,DEEAH^+/CO_3^=}$	-767.262
Salt-Molecules Parameters: $a_{c/a,m}$, $b_{c/a,m}$			
$a_{H_3O^+/OH^-,H_2O}$	-4*	$b_{H_3O^+/OH^-,H_2O}$	0*
$a_{H_3O^+/OH^-,CO_2}$	-8*	$b_{H_3O^+/OH^-,CO_2}$	0*
$a_{H_3O^+/OH^-,DEEA}$	3.7106	$b_{H_3O^+/OH^-,DEEA}$	-295.628
$a_{H_3O^+/HCO_3^-,H_2O}$	-4*	$b_{H_3O^+/HCO_3^-,H_2O}$	0*
$a_{H_3O^+/HCO_3^-,CO_2}$	-8*	$b_{H_3O^+/HCO_3^-,CO_2}$	0*
$a_{H_3O^+/HCO_3^-,DEEA}$	-1.3105	$b_{H_3O^+/HCO_3^-,DEEA}$	146.617
$a_{H_3O^+/CO_3^=,H_2O}$	-4*	$b_{H_3O^+/CO_3^=,H_2O}$	0*
$a_{H_3O^+/CO_3^=,CO_2}$	-8*	$b_{H_3O^+/CO_3^=,CO_2}$	0*
$a_{H_3O^+/CO_3^=,DEEA}$	-2.3338	$b_{H_3O^+/CO_3^=,DEEA}$	11.660
$a_{DEEAH^+/OH^-,H_2O}$	0.9263	$b_{DEEAH^+/OH^-,H_2O}$	-296.331
$a_{DEEAH^+/OH^-,CO_2}$	8.7102	$b_{DEEAH^+/OH^-,CO_2}$	-569.460
$a_{DEEAH^+/OH^-,DEEA}$	2.4086	$b_{DEEAH^+/OH^-,DEEA}$	605.016
$a_{DEEAH^+/HCO_3^-,H_2O}$	1.1823	$b_{DEEAH^+/HCO_3^-,H_2O}$	-46.530
$a_{DEEAH^+/HCO_3^-,CO_2}$	-7.6385	$b_{DEEAH^+/HCO_3^-,CO_2}$	200.853
$a_{DEEAH^+/HCO_3^-,DEEA}$	1.0199	$b_{DEEAH^+/HCO_3^-,DEEA}$	-126.497
$a_{DEEAH^+/CO_3^=,H_2O}$	-4.4225	$b_{DEEAH^+/CO_3^=,H_2O}$	-160.157

$a_{DEEAH^+/CO_3^=,CO_2}$	1.8621	$b_{DEEAH^+/CO_3^=,CO_2}$	-53.014
$a_{DEEAH^+/CO_3^=,DEEA}$	11.3149	$b_{DEEAH^+/CO_3^=,DEEA}$	-969.983

*Aspen default value

**Optimized in this work using unloaded DEEA system data

6. Conclusion

In this work experimental data for both unloaded and loaded aqueous DEEA solutions are presented. An equilibrium model is presented and non-idealities in the liquid phase are corrected by the e-NRTL model. The model is able to correlate with good accuracy the experimental data used in the regression. Moreover, it predicts reasonably well heat of absorption data which were not included in the regression.

Acknowledgements

Financial support from the EC 7th Framework Programme through Grant Agreement No: iCap-241391, is gratefully acknowledged

References

Aleixo, M., Prigent, M., Gibert, A., Porcheron, F., Mokbel, I., Jose, J., Jacquin, M., 2011. Physical and chemical properties of DMX™ solvents, pp. 148-155.

Austgen, D.M., Rochelle, G.T., Chen, C.C., 1991. Model of vapor-liquid equilibria for aqueous acid gas-alkanolamine systems. 2. Representation of hydrogen sulfide and carbon dioxide solubility in aqueous MDEA and carbon dioxide solubility in aqueous mixtures of MDEA with MEA or DEA. Industrial & Engineering Chemistry Research 30, 543-555.

Austgen, D.M., Rochelle, G.T., Peng, X., Chen, C.C., 1989. Model of vapor-liquid equilibria for aqueous acid gas-alkanolamine systems using the electrolyte-NRTL equation. Industrial & Engineering Chemistry Research 28, 1060-1073.

Carroll, J.J., Slupsky, J.D., Mather, A.E., 1991. The solubility of carbon dioxide in water at low pressure. J. Phys. Chem. Ref. Data 20, 1201-1209.

Chen, C.-C., Evans, L.B., 1986. A local composition model for the excess Gibbs energy of aqueous electrolyte systems. AIChE Journal 32, 444-454.

Ciftja, A.F., Hartono, A., Svendsen, H.F., 2013. Experimental study on phase change solvents in CO2 capture by NMR spectroscopy. Chemical Engineering Science 102, 378-386.

DIPPR, 2004. The DIPPR Informationand Data Evaluation Manager for the Design Institute for Physical Properties. Version 4.1.0.

Donaldson, T.L., Nguyen, Y.N., 1980. Carbon dioxide reaction kinetics and transport in aqueous amine membranes. Ind. Eng. Chem. Fundam. 19, 260-266.
Edwards, T.J., Maurer, G., Newman, J., Prausnitz, J.M., 1978. Vapor-liquid equilibria in multicomponent aqueous solutions of volatile weak electrolytes. AIChE Journal 24, 966-976.
Ghosh, S., Das, S., Kundu, D., Suresh, K., Abraham, A., 2012. Inter-particle communication and search-dynamics of lbest particle swarm optimizers: An analysis. Information Sciences 182, 156-168.
Hamborg, E.S., Versteeg, G.F., 2009. Dissociation Constants and Thermodynamic Properties of Amines and Alkanolamines from (293 to 353) K. Journal of Chemical & Engineering Data 54, 1318-1328.
Hartono, A., Saleem, F., Arshad, M.W., Usman, M., Svendsen, H.F., 2013. Binary and ternary VLE of the 2-(diethylamino)-ethanol (DEEA)/ 3-(Methylamino)-propylamine (MAPA)/ Water system. Submitted to Chemical Engineering Science.
Hessen, E.T., 2010. Thermodynamic models for CO_2 absorption, PhD Thesis. Department of Chemical Engineering. Norwegian University of Science and Technology, Trondheim.
Hessen, E.T., Haug-Warberg, T., Svendsen, H.F., 2010. The refined e-NRTL model applied to CO_2–H_2O–alkanolamine systems. Chem.Eng.Sci. 65, 3638-3648.
Kennedy, J., Eberhart, R., 1995. Particle swarm optimization, Neural Networks, 1995. Proceedings., IEEE International Conference on, pp. 1942-1948 vol.1944.
Kim, I., 2009. Heat of reaction and VLE of post combustion CO2 absorbents, PhD Thesis. Faculty of Natural Sciences and Technology, Department of Chemical Engineering. Norwegian University of Science and Technology, NTNU, Trondheim, Norway.
Kim, I., Hessen, E.T., Haug-Warberg, T., Svendsen, H.F., 2009. Enthalpies of absorption of CO2 in aqueous alkanolamine solutions from e-NRTL model. Energy Procedia 1, 829-835.
Kim, I., Svendsen, H.F., 2011. Comparative study of the heats of absorption of post-combustion CO_2 absorbents. International Journal of Greenhouse Gas Control 5, 390-395.
Liebenthal, U., Pinto, D.D.D., Monteiro, J.G.M.-S., Svendsen, H.F., Kather, A., 2013. Overall Process Analysis and Optimisation for CO_2 Capture from Coal Fired Power Plants based on Phase Change Solvents Forming Two Liquid Phases, GHGT11. Submitted to Energy Procedia, Kyoto, Japan.
Ma'mun, S., Jakobsen, J.P., Svendsen, H.F., Juliussen, O., 2005. Experimental and Modeling Study of the Solubility of Carbon Dioxide in Aqueous 30 Mass % 2-((2-Aminoethyl)amino)ethanol Solution. Ind. & Eng. Chem. Res. 45, 2505-2512.
Ma'mun, S., Nilsen, R.,Svendsen, H. F., and Juliussen, O., 2005. Experimental and Modeling Study of the Solubility of Carbon Dioxide in Aqueous 30 Mass % 2-((2-Aminoethyl)amino)ethanol Solution. Ind. & Eng. Chem. Res. 45, 2505-2512.
Mathonat, C., Maham, Y., Mather, A.E., Hepler, L.G., 1997. Excess Molar Enthalpies of (Water + Monoalkanolamine) Mixtures at 298.15 K and 308.15 K. Journal of Chemical & Engineering Data 42, 993-995.
Pinto, D.D.D., Monteiro, J.G.M.-S., Haug-Warberg, T., Svendsen, H.F., 2013. Fitting parameters in the e-NRTL model using the PSO algorithm. Submitted to Computers and Chemical Engineering.
Poli, R., Kennedy, J., Blackwell, T., 2007. Particle swarm optimization. Swarm Intelligence 1, 33-57.
Raynal, L., Alix, P., Bouillon, P.-A., Gomez, A., de Nailly, M.l.F., Jacquin, M., Kittel, J., di Lella, A., Mougin, P., Trapy, J., 2011. The DMX™ process: An original solution for lowering the cost of post-combustion carbon capture. Energy Procedia 4, 779-786.
Renon, H., Prausnitz, J.M., 1968. Local compositions in thermodynamic excess functions for liquid mixtures. AIChE Journal 14, 135-144.
Weiland, R.H., Chakravarty, T., Mather, A.E., 1993. Solubility of Carbon Dioxide and Hydrogen Sulfide in Aqueous Alkanolamines. Ind. Eng. Chem. 32, 1419-1430.

Yaws, C.L., Narasimhan, P.K., 2009. Chapter 1 - Critical properties and acentric factor—Organic compounds, in: Carl, L.Y. (Ed.), Thermophysical Properties of Chemicals and Hydrocarbons. William Andrew Publishing, Norwich, NY, pp. 1-95.